

tion for aspartic acid and attributed it to the effect of hydrogen bonds present in the crystal.

Our diffraction experiment results demonstrate that the combination of synchrotron primary radiation at a wavelength around $\lambda = 0.5 \text{ \AA}$ with a CCD area detector can provide a high-precision data set, suitable for accurate charge density determination in a few hours. The results obtained are comparable or even superior to those typically derivable from serial counter data. The short acquisition times open new perspectives for the application of the method on larger molecules of biological importance. In such cases, although the number of reflections increases drastically, there is almost no increase in the measuring time, if an area detector is used. Although the experimental conditions are not yet at an optimum, in the near future, the problems associated with the studies of large systems might be limited to the crystal size and quality rather than to the measuring time. Further improvements can be expected not only from developments in the intensity integration and data-processing strategies of the area detectors (18) but also from the intensity increase of synchrotron radiation sources in the next generation.

REFERENCES AND NOTES

1. R. F. W. Bader, *Atoms in Molecules, A Quantum Theory* (Clarendon, Oxford, 1990); R. F. W. Bader, P. Lode, A. Popelier, T. A. Keith, *Angew. Chem.* **106**, 647 (1994).
2. P. Politzer and D. G. Truhlar, *Chemical Applications of Atomic and Molecular Electrostatic Potentials* (Plenum, New York, 1981).
3. B. M. Craven and P. Benci, *Acta Crystallogr. Sect. B* **37**, 1584 (1981); C. Lecomte, M. Souhassou, N. Ghermani, V. Pichon-Pesme, N. Bouhaida, *Trans. Am. Crystallogr. Assoc.* **V 26**, 55 (1990).
4. P. Coppens, *X-ray Charge Densities and Chemical Bonding* (Oxford Science, Oxford, 1997).
5. P. Coppens, *Science* **158**, 1577 (1967); R. F. Stewart, *J. Chem. Phys.* **51**, 4569 (1969).
6. C. Gatti, R. Bianchi, R. Destro, F. Merati, *J. Mol. Struct. (Theochem.)* **255**, 409 (1992); C. Flensburg, S. Larsen, R. F. Stewart, *J. Phys. Chem.* **99**, 10130 (1995); T. Koritsánszky, J. Buschmann, P. Luger, *ibid.* **100**, 10547 (1996).
7. The resolution of the diffraction experiment is defined by $d = \lambda/2\sin\theta$, where θ is the scattering angle and λ is the wavelength of the radiation.
8. A. Darovsky, R. Bolotovskiy, V. Kezerashvili, P. Coppens, *Acta Crystallogr. Sect. A* **52**, C-547 (1996); M. Carducci, R. Bolotovskiy, P. Coppens, *ibid.*, p. C-342.
9. DL-Proline, the racemic mixture of the naturally occurring amino acid proline, crystallizes as a monohydrate in an orthorhombic cell. The space group symmetry is *Pbca*, and the unit cell is defined by the lattice constant vectors of length $a = 5.253(3) \text{ \AA}$, $b = 11.987(5) \text{ \AA}$, and $c = 19.864(10) \text{ \AA}$. (The numbers in parentheses refer to errors in the last digit.)
10. N. K. Hansen and P. Coppens, *Acta Crystallogr. Sect. A* **34**, 909 (1978).
11. T. Koritsánszky *et al.*, *XD—A Computer Program Package for Multipole Refinement and Analysis of Electron Densities from Diffraction Data* (User Manual, Free University of Berlin, Berlin, 1995).
12. E. Clementi and C. Roetti, *At. Data Nucl. Data*

Tables **14**, 177 (1974).

13. M. J. Frisch *et al.* Gaussian 92/DFT, Revision G.1 (Gaussian Inc., Pittsburgh, PA, 1993).
14. It is an ab initio molecular orbital calculation at the Hartree-Fock level of approximation based on the use of Gaussian basis functions. The 6-311++G(3df,3pd) is a triple-zeta basis set and includes diffuse and high-angular momentum functions. This is the most extended standard basis set available in the Gaussian program system.
15. R. Flaig, T. Koritsánszky, D. Zobel, P. Luger, *J. Am. Chem. Soc.*, in press.
16. G. Khanarian and W. J. Moore, *Aust. J. Chem.* **33**, 1727 (1980).

17. Z. W. Su and P. Coppens, *Acta Crystallogr. Sect. A* **48**, 188 (1992).
18. R. Bolotovskiy, M. A. White, A. Darovsky, P. Coppens, *J. Appl. Crystallogr.* **28**, 86 (1995).
19. E. Keller, SCHAKAL88: User manual (University of Freiburg, Freiburg, Germany, 1988).
20. Funded by the Bundesminister für Bildung, Wissenschaft, Forschung und Technologie, Bonn, Germany (grant 05 647KEA1), and by the Fonds der Chemischen Industrie, Frankfurt, Germany. We thank B. Dittrich for preparing crystals suitable for the experiment.

14 October 1997; accepted 2 December 1997

Space Geodetic Observations of Nazca–South America Convergence Across the Central Andes

Edmundo Norabuena, Lisa Leffler-Griffin, Ailin Mao, Timothy Dixon, Seth Stein,* I. Selwyn Sacks, Leonidas Ocola, Michael Ellis

Space geodetic data recorded rates and directions of motion across the convergent boundary zone between the oceanic Nazca and continental South American plates in Peru and Bolivia. Roughly half of the overall convergence, about 30 to 40 millimeters per year, accumulated on the locked plate interface and can be released in future earthquakes. About 10 to 15 millimeters per year of crustal shortening occurred inland at the sub-Andean foreland fold and thrust belt, indicating that the Andes are continuing to build. Little (5 to 10 millimeters per year) along-trench motion of coastal forearc slivers was observed, despite the oblique convergence.

The high peaks and volcanoes of the Andes and the great earthquakes along the South American coast are dramatic manifestations of ocean-continent plate convergence because the oceanic Nazca plate subducts beneath South America. Convergence occurs over a 500- to 1000-km-wide boundary zone, within which several styles of deformation play a major role in the evolution of the South American continent (1).

We studied this convergence using space-based geodetic techniques: the global positioning system (GPS), Satellite Laser Ranging (SLR), and the Doppler Orbitography and Radiopositioning Integrated Satellite System (DORIS). These techniques combine precise satellite-based timing,

ranging, and orbit estimation to measure the positions of geodetic monuments to centimeter or better accuracy, such that measurements over time yield precise relative velocities (2).

The total relative plate motion is thought to be partitioned into several components (Fig. 1). Some motion accumulates on locked portions of the plate interface at the trench, causing transient elastic deformation, and is released when the interface ruptures in large thrust earthquakes (3). Some motion would be expected to occur by stable sliding at the interface, because the slip rate from large subduction zone earthquakes is typically less than the plate motion (4). The Andes and their thick crustal root (5) suggest that some of the motion causes permanent deformation through crustal shortening and mountain building. Geological studies and seismicity suggest that the high Altiplano plateau should be largely stable and that shortening by thrust faulting and folding occurs in the sub-Andean foreland fold and thrust belt to the east (6, 7). In addition, because convergence is oblique to the trench through much of the region, some trench-parallel motion of coastal forearc slivers might be expected (8).

Using space geodesy, we observed the motion of sites within a section across the plate boundary zone. We used GPS to mon-

E. Norabuena, Instituto Geofísico del Perú, Apartado 3747, Lima 100, Perú, and Rosenstiel School for Marine and Atmospheric Sciences, University of Miami, 4600 Rickenbacker Causeway, Miami, FL 33149, USA.

L. Leffler-Griffin and S. Stein, Department of Geological Sciences, Northwestern University, Evanston, IL 60208, USA.

A. Mao and T. Dixon, Rosenstiel School for Marine and Atmospheric Sciences, University of Miami, 4600 Rickenbacker Causeway, Miami, FL 33149, USA.

I. S. Sacks, Department of Terrestrial Magnetism, Carnegie Institute of Washington, 5241 Broad Branch Road, NW, Washington, DC 20015, USA.

L. Ocola, Instituto Geofísico del Perú, Apartado 3747, Lima 100, Perú.

M. Ellis, Center for Earthquake Research and Information, University of Memphis, TN 38152, USA.

*To whom correspondence should be addressed.

itor geodetic monuments in Peru and Bolivia installed for this purpose and occupied in 1994 and 1996 as part of the South America–Nazca Plate Project (Figs. 1 and 2) (9). Some Bolivian sites were also occupied in 1995. We also used continuously recording GPS sites in the interior of South America and the Nazca plate, SLR data from Easter Island, and DORIS data from Easter and Galápagos islands. Although most sites were only occupied twice, the minimum necessary to define velocities, the other sites gave virtually identical velocities regardless of whether the 1995 data were used, suggesting that horizontal velocities for sites with two occupations are not unduly biased compared with those with three. Independent estimates for Arequipa, from more than a decade of SLR data and more than 3 years of daily GPS data, match our results near this site within errors. We did not use the vertical components, which have larger uncertainties.

To define site velocities relative to stable South America, we used data from four permanent GPS sites in stable South America and our two eastern survey sites (RBLT and SJCH) to estimate a South America Euler vector (10). We then characterized Nazca plate motion using data from islands on the plate. Several years of SLR, GPS, and DORIS data from Easter Island gave a weighted mean velocity with respect to stable South America of 75 ± 5 mm/year directed N106°E, which is slower than that predicted by NUVEL-1A (80 ± 2 mm/year directed N99°E). All three techniques yielded vectors that are slower than the NUVEL-1A prediction and rotated clockwise from it (Fig. 1), suggesting that the discrepancy may be real (11, 12). These data and data from Galápagos allowed estimation of a Nazca plate Euler vector (13). Unfortunately, there are no SLR data from Galápagos, and GPS and DORIS data there span a short time, limiting the precision of the velocity estimate. The resulting Nazca–South America Euler vector predicts convergence at the trench (17°S, 75°W) of 68 mm/year directed N76°E, which is 12% slower than the NUVEL-1A prediction of 77 mm/year at N79°E.

Site velocities relative to stable South America (Figs. 2 and 3) decreased from the interior of the Nazca plate to the interior of South America. Because the width of the Altiplano varies, we divided the data into groups north and south of a profile normal to the trench at 17°S and modeled these processes using the boundary element program 3D-

DEF (14). Subduction-related strain between earthquakes was modeled by reverse slip on the locked or partially locked plate interface (3), an approach used for analysis of similar GPS data elsewhere (15). The slip rate locked on the interface should be released in subsequent earthquakes and thus ideally would correspond to the seismically estimated slip rate. Because (as discussed later) these two need not be the same, we avoid the terms “seismic” or “aseismic” slip rates for geodetically estimated quantities.

The predicted velocities near the trench

depend on the geometry of the subduction zone, which we constrained from seismological results in the general area (16). We modeled the locked portion of the interface as three segments with progressively steeper dips: 10° to 15-km depth, 18° from 15- to 35-km depth, and 26° from 35- to 50-km depth. Varying the dip within 3° and the locking depth within 5 km changed the predicted deformation field by less than the observational errors.

We interpret the data as indicating that only part of the interplate slip is locked on

Fig. 1. Geometry of the Nazca–South America plate boundary zone, together with GPS, DORIS, and SLR site velocities used to estimate Nazca and South America plate motions. Velocities are relative to stable South America, and ellipses show 95% confidence limits. EISL, Easter Island; GALA, Galápagos. Box shows the area of Fig. 2.

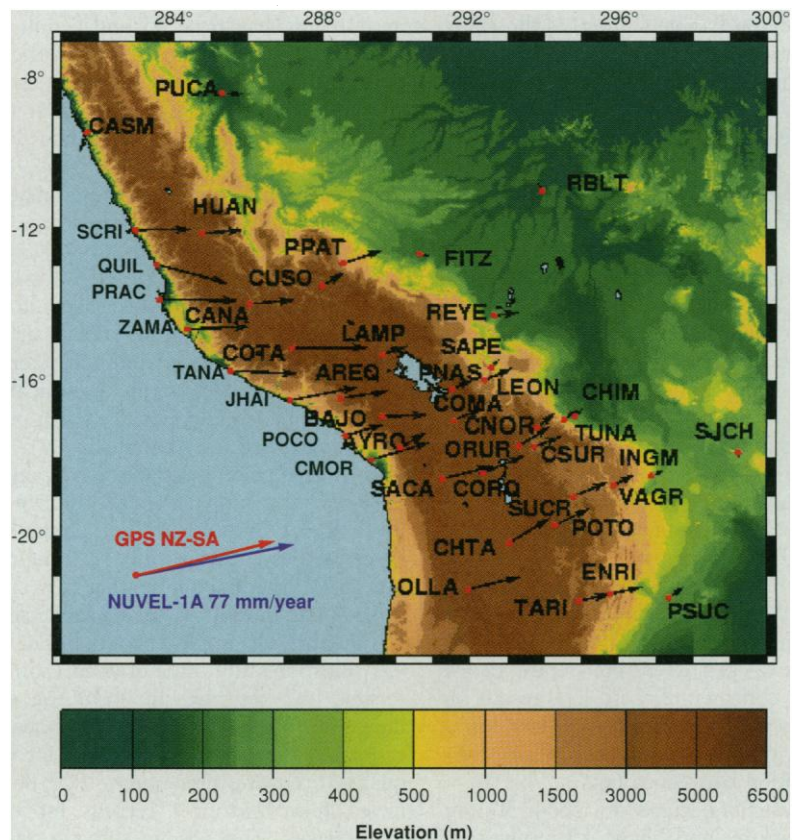
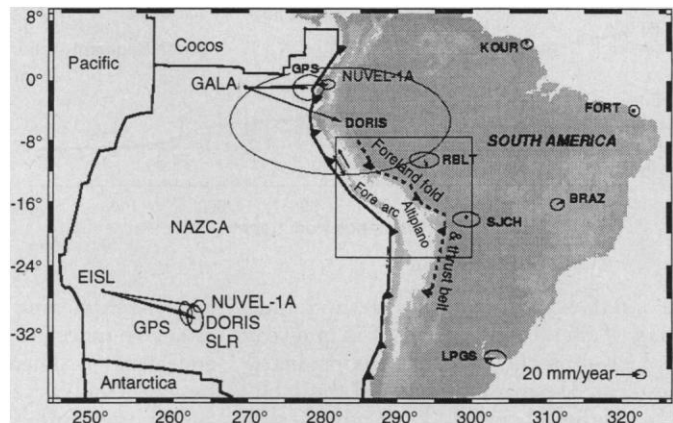


Fig. 2. Global positioning system–derived velocities relative to stable South America (SA) from sites in the survey, compared with convergence velocities predicted by NUVEL-1A and the plate-wide space geodetic data (Fig. 1). NUVEL-1A vector gives rate scale. NZ, Nazca.

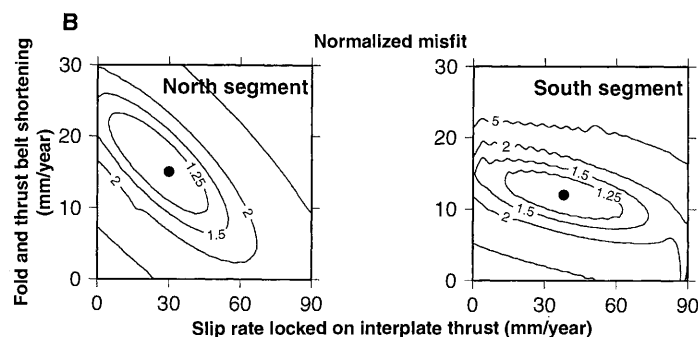
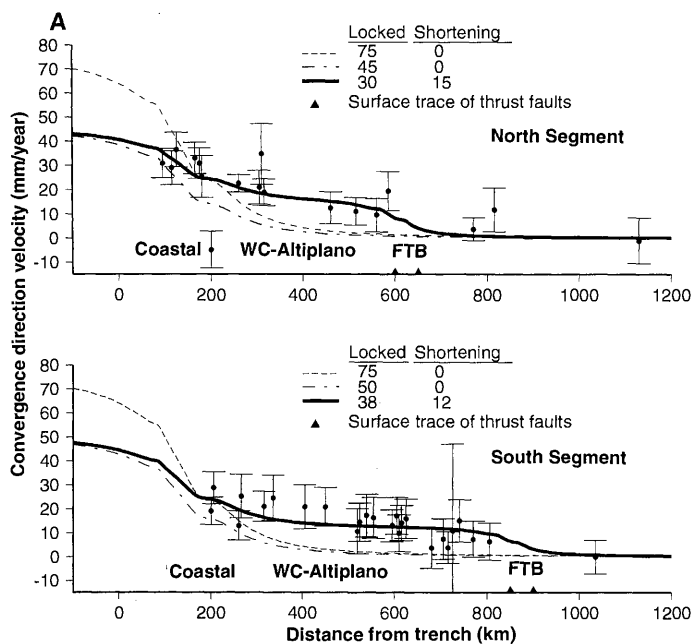


Fig. 3. (A) Velocity of GPS sites in the direction parallel to NUVEL-1A convergence direction, with error bars (95% confidence). Panels show profiles for north (top) and south (bottom) site groups. Solid lines show the predicted velocity for the best fitting models, in which only some of the predicted convergence is locked at the plate interface and shortening occurs in the eastern Andes. Short dashed lines show predictions of models with all the predicted convergence locked on the plate interface and no shortening. Long-short dashed lines show predictions of models with no shortening and locking on the plate interface equal to the sum of the locking and shortening in the best fitting model. (B) Contour plots showing χ^2 misfits to the data in each profile, as a function of the slip rate locked on the plate boundary and the shortening rate. Best fits are shown by dots.

the interface and that crustal shortening occurs. If a total convergence of 75 mm/year was locked on the interface, the predicted rates (Fig. 3) generally exceeded those observed within about 150 km of the trench (north profile) but were less than those observed at a greater distance. The effect of partial locking (stable sliding) is illustrated by the curves in Fig. 3, which were computed with the assumption that only part of the total convergence, 45 mm/year (north) and 50 mm/year (south), locks the fault. The predicted rates near the trench were smaller and fit the data better, because only the portion of the slip locked at the interface produces transient deformation. Farther than about 300 km from the trench, however, a misfit remained.

We modeled the remaining misfit by including shortening in the eastern Andes. Although some shortening may occur by seismic strain accumulation and release, we assumed that most of it reflects a permanent change in the position of Andean crust with respect to stable South America. On the basis of geological data, we modeled convergence with thrust faults (Fig. 3) 600 to 650 km from the trench for the north profile and 850 to 900 km from the trench for the south profile. The faults were assumed to dip 30°W and to be locked to 20-km depth, typical values for continental crust. The results are largely insensitive to the precise location of the faults, their geometry, and the partitioning of motion between them.

The best fits occurred for about 30 mm/year of locking and about 15 mm/year of shortening on the northern profile and for about 38 mm/year of locking and about 12 mm/year of shortening on the southern pro-

file. The shortening and locking rates can be estimated independently because they influence data at different distances from the trench. Thus, we can discriminate models with the best fitting locked and the shortening rate from models with a locked rate equal to their sum and no shortening (that is, 30 and 15 mm/year from 45 and 0 mm/year). These estimates do not depend on the total convergence rate because they were estimated directly from the geodetic data, rather than as differences from an assumed total convergence.

For the northern profile, the estimated 30 mm/year of locked slip accumulating on the plate interface corresponds to 39% of the convergence predicted by NUVEL-1A or 44% of that predicted by space geodesy. Subtracting 15 mm/year of Andean shortening implies that the remaining 42% or 34% of the plate motion occurs aseismically by smooth stable sliding. For the south profile, the estimated 38 mm/year of slip accumulating on the plate interface corresponds to 49% of the convergence predicted by NUVEL-1A or 56% of that predicted by space geodesy. Subtracting 12 mm/year of Andean shortening implies that 35% or 26% of the plate motion occurs by stable sliding.

These results are interesting because this area illustrates the difficulties in estimating seismic and aseismic slip from the earthquake record (4). Slip in past earthquakes is estimated from seismological data for earthquakes occurring after circa 1900 and inferred from historical records for earlier earthquakes. The seismic slip rate is then inferred from earthquake history and compared with a plate motion model. This process has several limitations. Uncertainties in

estimating source parameters of earthquakes from historical data are considerable (17), the seismic cycle is typically longer than the instrumental record (18), and the size and recurrence interval of earthquakes on a trench segment can be variable (17, 19, 20). Some large earthquakes have substantial slow afterslip (21) not included in the seismic moment calculation, which produces a spurious seismic slip deficit. Hence, it is difficult to assess whether an apparent seismic slip deficit indicates a seismic gap where large earthquakes are overdue or that much of the interplate motion occurs aseismically (22). Estimation of aseismic slip compounds the uncertainty, because the estimated seismic slip is subtracted from an assumed convergence rate, so different plate motion models give different results (19). Moreover, crustal shortening (about 15% of net convergence here) is typically not subtracted from the assumed convergence.

The use of GPS data reduced these uncertainties because we more directly estimated the total plate motion, shortening rate, and locked slip rate accumulation, regardless of whether the latter would be released in a conventional earthquake or afterslip. However, the GPS data faced the difficulty of accounting for possible deformation of the upper plate due to strain diffusion for tens to hundreds of years after large earthquakes (23). Extended periods of data will be needed to see how substantial this effect is.

The GPS results suggest that about 15 mm/year of shortening occurs in the fold and thrust belt. A lower estimate, 1 to 3 mm/year, comes from the seismic moments of earthquakes (6). Geologic shortening estimates range from 8 to 13 mm/year aver-

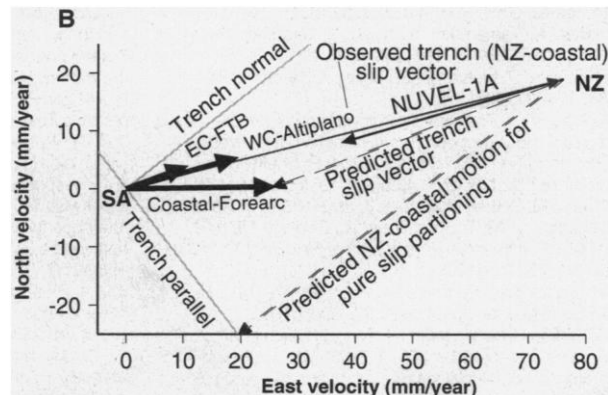
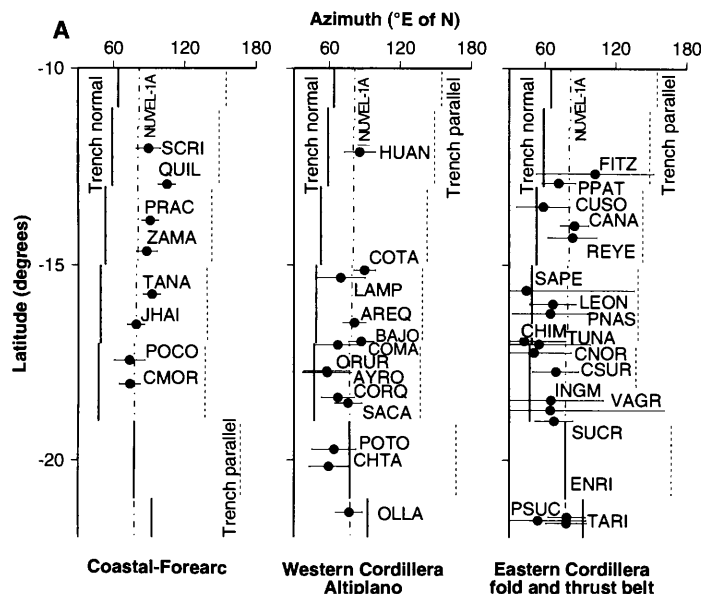


Fig. 4. (A) Global positioning system–derived site motion azimuths relative to stable South America, with 95% confidence limits, as a function of latitude, for sites in three groups. Also shown are the convergence azimuth predicted by NUVEL-1A and the trench-normal and trench-parallel directions. (B) Average velocity for these groups, relative to stable South America, trench slip vector direction predicted by coastal site motions, and observed trench slip vector direction. WC, Western Cordillera; EC, Eastern Cordillera; FTB, fold and thrust belt.

aged over the post-Oligocene [past 25 million years (My)] to 27 mm/year averaged over the past 5 My (7). Thus, our GPS estimates, and less precise estimates derived with only one permanent GPS site (24), are comparable with geological estimates made with the assumption of constant post-Oligocene shortening. Although more complicated scenarios are possible (rapid initial shortening followed by lower rates), the simplest interpretation is that crustal thickening has been building the high Andes by thrust faulting and folding at an approximately steady rate for about 25 My, as the deformation, now at the sub-Andean fold and thrust belt, migrated eastward (7). Perhaps in plate boundary zones, both the overall plate motion and its different components remain approximately constant over long periods even when the geometry changes (thrusting stepping eastward). Similar observations have been made for components of the San Andreas system (25).

The observation that the geodetic and geologic shortening estimates exceed the seismic estimate implies that most shortening either occurs aseismically or (less likely) will be released in future earthquakes. Other continental areas offer little guidance: in some areas, seismic strain rates match the expected relative motion, but a deficit exists in others (26), although the geodetically and seismically inferred deformation is similarly oriented (27).

We used the data to test for slip partitioning, a phenomenon that occurs in some situations in which convergence is oblique to the trench (8). In such situations, earthquake slip vectors at the trench are often rotated from the predicted convergence direction toward the trench-normal direction,

reflecting thrust faulting between the subducting plate and a forearc sliver, and strike-slip motion is expected between the forearc and the interior of the overriding plate. The motion of the northern coastal sites relative to South America (Fig. 4) is rotated about 10° from the convergence direction, indicating slightly (about 5 mm/year) more trench-parallel motion than expected from the decomposition of a vector of this length in the convergence direction. This motion implies that the coastal sites move about 8 mm/year left laterally in the trench-parallel direction, relative to the Western Cordillera and Altiplano sites.

It is unclear whether this small motion is significant, and if so, whether it reflects permanent trench-parallel transport of a coastal sliver or transient forearc deformation due to the seismic cycle that will be released in future large earthquakes. The present GPS data are insufficient to show directly coastal motion with respect to the Western Cordillera and Altiplano sites. Similarly, the expected deviation in the trench slip vectors is difficult to assess. This motion can be predicted with analysis in velocity space (Fig. 4), although the observed site motions include the transient effects of the seismic cycle. The observed motion of the coastal sites relative to stable South America predicts Nazca–coastal forearc motion trending about $N70^\circ E$, between the plate motion and trench-normal directions. The mean direction of slip vectors at the trench is rotated somewhat from the predicted convergence direction, to about $N74 \pm 4^\circ E$. However, given the scatter in slip vectors and the uncertainties in the GPS data and in NUVEL-1A, it is difficult to draw a definite conclusion.

The azimuthal deviation from the con-

vergence direction varies with latitude. Northern coastal sites show some, whereas those to the south near the bend in the coastline at $18^\circ S$, where the obliquity changes, show essentially none. If this correlation is not accidental, the subduction geometry affects either the interseismic elastic strain or the sliver motion. If the latter is the case, the small slip partitioning may reflect the force balance between the thrust and strike-slip faults (8), with additional resistance to strike slip provided by the “buttress effect” (28) of the bend.

Our initial results, which will be refined by subsequent data, and studies elsewhere illustrate how space-based geodesy is opening a new era for studies of plate convergence and continental mountain building (29). We are approaching the point at which understanding of the convergence process will no longer be limited by the kinematic data.

REFERENCES AND NOTES

1. J. Dewey and S. Lamb, *Tectonophysics* **205**, 79 (1992).
2. GPS techniques are reviewed by T. Dixon [*Rev. Geophys.* **29**, 249 (1991)]. For information on DORIS, see A. Cazenave, J. Valette, and C. Boucher [*J. Geophys. Res.* **97**, 7109 (1992)]. SLR is summarized by D. Smith *et al.* [*ibid.* **95**, 22013 (1990)]. For tectonic applications of space geodesy, see R. G. Gordon and S. Stein [*Science* **256**, 333 (1992)] and S. Stein [*in Space Geodesy and Geodynamics*, D. Smith and D. Turcotte, Eds. (American Geophysical Union, Washington, DC, 1993), pp. 5–20].
3. J. C. Savage, *J. Geophys. Res.* **88**, 4984 (1983).
4. H. Kanamori, in *Island Arcs, Trenches and Back-Arc Basins*, M. Talwani and W. Pitman III, Eds. (American Geophysical Union, Washington, DC, 1977), pp. 163–174; K. McNally and J. Minster, *J. Geophys. Res.* **86**, 4949 (1981); E. Peterson and T. Seno, *ibid.* **89**, 10233 (1984); J. Pacheco, L. Sykes, C. Scholz, *ibid.* **98**, 14133 (1993).

5. D. James, *Geol. Soc. Am. Bull.* **82**, 3325 (1971); Y. Fukao, A. Yamamoto, M. Kono, *J. Geophys. Res.* **94**, 3876 (1989); B. Isacks, *ibid.* **93**, 3211 (1988).
6. G. Suarez, P. Molnar, B. Burchfiel, *J. Geophys. Res.* **88**, 10403 (1983).
7. F. Megard, in *The Anatomy of Mountain Ranges*, J. Schnaer and J. Rogers, Eds. (Princeton Univ. Press, Princeton, NJ, 1987), pp. 179–204; B. Sheffels, *Geology* **18**, 812 (1990); M. Schmitz, *Tectonics* **13**, 484 (1994); M. Sebrier *et al.*, *ibid.* **7**, 895 (1988); D. Roeder, *ibid.*, p. 23; T. Sempere *et al.*, *Geology* **18**, 946 (1990); R. Allmendinger *et al.*, *Annu. Rev. Earth Planet. Sci.* **25**, 139 (1997).
8. M. Beck, *Phys. Earth Planet. Inter.* **68**, 1 (1991); R. McCaffrey, *J. Geophys. Res.* **97**, 8905 (1992).
9. GPS data were analyzed following T. Dixon *et al.* [*J. Geophys. Res.* **102**, 12017 (1997)]. We used high-precision nonfiducial satellite orbits and the Jet Propulsion Laboratory GIPSY analysis software to estimate site velocities in the International Terrestrial Reference Frame (ITRF-94) reference frame (10). Site velocities were estimated from least squares fits to daily positions weighted by the scaled formal error. Data from one site (CASM, Fig. 2) were anomalous, perhaps because of errors in setting up the GPS antenna over the geodetic monument. Sites, data, and uncertainties are given at www.sciencemag.org/feature/data/975403.shl
10. Plate motions are specified by Euler (angular velocity) vectors giving either the relative motion between a plate pair or the absolute motion of an individual plate. These vectors can now be derived from space geodetic data and were previously derived from data recording plate motions averaged over the past few million years [C. Chase, *Geophys. J.* **29**, 117 (1972); J. Minster *et al.*, *ibid.* **36**, 541 (1974)]. ITRF-94, a reference frame for space geodetic data [C. Boucher, *IERS Technical Note 20* (Observatoire de Paris, Paris, 1996)], is designed to agree on average with the absolute plate motion model NNR NUVEL-1A, termed NNR-A. The latter is a revision of model NNR, derived by combining the assumption of no net torque on the lithosphere [D. Argus and R. Gordon, *Geophys. Res. Lett.* **18**, 2039 (1991)] with global relative plate motion model NUVEL-1 [C. DeMets *et al.*, *Geophys. J. Int.* **101**, 425 (1990)], reflecting a change in the magnetic anomaly time scale subsequent to the publication of NUVEL-1. NUVEL-1A and NNR-A predict plate motion directions identical to those for NUVEL-1 and NNR NUVEL-1, but 4% slower [C. DeMets *et al.*, *Geophys. Res. Lett.* **21**, 2191 (1994)]. Because rate data in the models come from ridges, the predicted rates across subduction zones are derived indirectly by the closure of plate circuits. Space geodetic velocities in ITRF-94 can be compared with plate motions predicted by NNR-A, and relative motions are typically compared with NUVEL-1A (30).
11. J. Robbins, D. Smith, and C. Ma [in *Space Geodesy and Geodynamics*, D. Smith and D. Turcotte, Eds. (American Geophysical Union, Washington, DC, 1993), pp. 21–36] noted the discrepancy at Easter Island between the motion estimated from SLR and that predicted by NUVEL-1A. However, data at one site provide only the two horizontal velocity components and are hence insufficient to define the three components of the Nazca plate's angular velocity vector, which requires horizontal velocity measurements at two sites (30).
12. Space geodetic data for plate motions over a few years generally agree surprisingly well with the predictions of global plate motion models derived by estimating plate motions over millions of years (2, 11, 30). However, changes in plate motions over the past 3 My have been suggested for other plate pairs both from GPS data (30) and magnetic anomalies [C. DeMets, *Geophys. Res. Lett.* **22**, 3545 (1995)]. Because our Nazca–South America Euler vector was derived from a short time series at only two sites, it is unclear whether importance should be ascribed to the discrepancy between it and the vector from NUVEL-1A. The discrepancy may reflect the limited data, NUVEL-1's derivation without direct data across the subduction zone, or a change in plate motions. Assessment of such possible changes should improve as additional space geodetic sites and longer time series become available.
13. For the permanent sites in South America, we used the data available since 1 August 1994: 3 years at KOUR and FORT, 2 at BRAZ, and 1.5 at LPGS. The resulting Euler vector in ITRF-94 has pole at 21.63°S, 154.22°W; magnitude of 0.134°/My; an error ellipse with major (σ_{\max}) and minor (σ_{\min}) axes 16.6° and 4.4°, respectively; a major axis oriented –78.5° [clockwise from north (cw from N)]; and a rotation rate uncertainty (σ_{ω}) of 0.012°/My. The Nazca plate data yield a Euler vector in ITRF-94 [pole at 34.32°N, 101.12°W; magnitude, 0.735°/My; σ_{\max} , 3.62°; σ_{\min} , 0.7°; azimuth, –4° (cw from N); and σ_{ω} , 0.03°/My] and hence a Nazca–South America relative Euler vector with pole at 40.58°N, 90.52°W, magnitude of 0.713°/My; and uncertainties σ_{\max} , 4.4°; σ_{\min} , 2.2°; azimuth, –7.4° (cw from N), and σ_{ω} , 0.03°/My.
14. J. Gombert and M. Ellis, *J. Geophys. Res.* **99**, 20299 (1994).
15. T. Dixon, *Geophys. Res. Lett.* **20**, 2167 (1993).
16. B. Tichelaar and L. Ruff, *J. Geophys. Res.* **96**, 11997 (1991).
17. S. Nishenko, *Pure Appl. Geophys.* **135**, 169 (1991). For the recurrence intervals estimated in this paper, application of earthquake scaling relations [R. Geller, *Bull. Seismol. Soc. Am.* **66**, 1501 (1976)] implies seismic slip rates of about 10 to 20 mm/year between 16° and 14°S.
18. R. McCaffrey, *Bull. Seismol. Soc. Am.* **87**, 1069 (1997).
19. S. Stein *et al.*, *Geophys. Res. Lett.* **13**, 713 (1986).
20. W. Thatcher, *J. Geophys. Res.* **95**, 2609 (1990).
21. H. Kanamori and J. Cipar, *Phys. Earth Planet. Inter.* **9**, 128 (1974); I. Clifuentes and P. Silver, *J. Geophys. Res.* **94**, 643 (1989); S. Barrientos, *Geophys. Res. Lett.* **22**, 3541 (1995); K. Heki, S. Miyazaki, H. Tsuji, *Nature* **386**, 595 (1997).
22. The question may be analogous to deciding whether bear attacks being more common in Wyoming than in New York indicates a “gap” where attacks are overdue or a difference in intrinsic hazard [S. Stein, *Nature* **356**, 387 (1992)].
23. P. Rydelek and S. Sacks, *Geophys. J. Int.* **100**, 39 (1990); F. Pollitz, *J. Geophys. Res.* **102**, 17921 (1997).
24. L. Leffler *et al.*, *Geophys. Res. Lett.* **24**, 1031 (1997).
25. K. Feigl *et al.*, *J. Geophys. Res.* **98**, 21677 (1993); T. Dixon *et al.*, *Tectonics* **14**, 755 (1995).
26. J. Jackson, J. Haines, W. Holt, *J. Geophys. Res.* **100**, 15205 (1995); K. Abdrakhmatov *et al.*, *Nature* **384**, 450 (1996).
27. J. Jackson, J. Haines, W. Holt, *Geophys. Res. Lett.* **21**, 2849 (1994).
28. M. Beck *et al.*, *Tectonics* **13**, 215 (1994).
29. J. Freymueller, J. Kellogg, V. Vega, *J. Geophys. Res.* **98**, 21853 (1993); M. Bevis *et al.*, *Nature* **374**, 249 (1995); J. Freymueller *et al.*, *Geophys. Res. Lett.* **23**, 3107 (1996); R. Bilham *et al.*, *Nature* **386**, 61 (1997); R. King *et al.*, *Geology* **25**, 179 (1997). Global positioning system programs are also acquiring data in Chile and Argentina, south of our survey area.
30. D. Argus and M. Heflin, *Geophys. Res. Lett.* **22**, 1973 (1995); T. Dixon and A. Mao, *ibid.* **24**, 535 (1997); K. Larson, J. Freymueller, S. Philipson, *J. Geophys. Res.* **102**, 9961 (1997).
31. Supported by NASA's Geodynamics program and NSF's Small Grants for Exploratory Research program. We thank the Instituto Geografico Militar, Bolivia, the Instituto Geofisico del Peru, and University Navstar Consortium (especially J. Richardson, B. Baker, and K. Feaux) for invaluable assistance in GPS campaigns; J. Lee and V. Berhow for assistance with site selection; S. Wdowinski, R. Russo, C. DeMets, and R. McCaffrey for helpful discussions; and the international geodetic community for maintaining a permanent GPS network with publicly available data.

3 October 1997; accepted 26 November 1997

A Search for Endogenous Amino Acids in Martian Meteorite ALH84001

Jeffrey L. Bada,* Daniel P. Glavin, Gene D. McDonald, Luann Becker

Trace amounts of glycine, serine, and alanine were detected in the carbonate component of the martian meteorite ALH84001 by high-performance liquid chromatography. The detected amino acids were not uniformly distributed in the carbonate component and ranged in concentration from 0.1 to 7 parts per million. Although the detected alanine consists primarily of the L enantiomer, low concentrations (<0.1 parts per million) of endogenous D-alanine may be present in the ALH84001 carbonates. The amino acids present in this sample of ALH84001 appear to be terrestrial in origin and similar to those in Allan Hills ice, although the possibility cannot be ruled out that minute amounts of some amino acids such as D-alanine are preserved in the meteorite.

The report by McKay *et al.* (1) that the martian meteorite ALH84001 contains evidence of biological processes on Mars remains controversial. Of central importance

is whether ALH84001 contains endogenous organic compounds, and if so, whether these compounds are biological or abiotic in origin. The bulk meteorite is reported to contain 100 to 200 parts per million (ppm) of combustible carbon (2), supposedly derived from organic compounds. So far, however, the only specific compounds that have been reported are parts per million amounts of polycyclic aromatic hydrocarbons (PAHs) detected in the carbonate globule component of the meteorite (1). Another martian meteorite collected in the Antarctic

J. L. Bada and D. P. Glavin, Scripps Institution of Oceanography, University of California at San Diego, La Jolla, CA 92093-0212, USA.

G. D. McDonald, Jet Propulsion Laboratory MS 183-301, 4800 Oak Grove Drive, Pasadena, CA 91109, USA.

L. Becker, Hawaii Institute of Geophysics and Planetology, University of Hawaii at Manoa, Honolulu, HI 96822, USA.

*To whom correspondence should be addressed. E-mail: jbada@ucsd.edu